FINAL ADMINSTRATIVE REPORT

Title: Presidential Young Investigator Award: Continuum Vibrations and Buckling of 2-D and 3-D Structural Bodies

Sponsor: National Science Foundation

University: Georgia Institute of Technology

Project Director: Oliver O. McGee

GT P/S Project No.: 1606P11

GT Old Project No: E-16-P11

Contract No.: CMS-9618308

Date: February 10, 2004

Vibration of Plates with Constrained V-Notches or Cracks

O. G. McGee[1]; A. W. Leissa[2]; J. W. Kim[3]; and Y. S. Kim[4]

Abstract: This paper reports the first known free vibration solutions for thin circular plates with V-notches having various edge conditions. The classical Ritz method is employed with two sets of admissible functions assumed for the transverse vibratory displacements. These sets include: (1) mathematically complete algebraic-trigonometric polynomials which guarantee convergence to exact frequencies as sufficient terms are retained; and (2) corner functions which account for the bending moment singularities at the sharp re-entrant corner of the V-notch. Extensive convergence studies summarized herein confirm that the corner functions substantially enhance the convergence and accuracy of nondimensional frequencies for circular plates having a free circumferential edge and various combinations edge conditions of the V-notch. Accurate (five significant figures) frequencies are presented for clamped-free, clamped-hinged, and hinged-free notches for the spectra of notch angles (1°,5°,10°,30°,60°,90°), causing a re-entrant vertex corner of the radial edges. For very small notch angles, a *clamped-free, clamped-hinged,* or *hinged-free* radial crack ensues. One general observation is that, for the range of notch angles considered, there is a substantial increase in the first six frequencies as the notch depth increases. The frequency increase with increasing notch depth is more pronounced in the higher modes than the lower ones, and is quite substantial for segmental plates with notch angles equal to 180°. A large reduction in frequencies is also observed as the notch angle decreases at a constant notch depth. A new database of accurate frequencies and mode shapes for sectorial, semicircular and segmental plates is presented with which future solutions drawn from alternative numerical procedures and finite element and boundary element techniques may be compared. Normalized contours of the transverse vibratory displacement are shown for plates with various notch depths and notch angles of 5°, 30°, 60°, 90°, and 180°.

DOI: 10.1061/(ASCE)0733-9399(2003)129:7(812)

CE Database subject headings: Plates; Vibration; Displacement.

Introduction

Documented in a summarizing monograph (Leissa 1969) and a series of review articles (Leissa 1977, 1981, 1987) are hundreds of technical publications explicating the free vibration characteristics of complete circular and annular plates with various support conditions along the circumferential boundaries or at interior points. The scope of vibration publications has been extended to annular plates having nonconcentric interior circumferential boundaries (Nagaya 1977, 1979; Eastep and Hemming 1978; Khurasia and Rawtani 1978) and to plates having doubly connected arbitrary shape (Nagaya 1981, 1983). Collectively, these publications provide one with a perspective of the need for new information on the title problem in the vibration literature.

Accurate (at least four significant figures) frequencies and mode shapes have been reported in some recent work on circular plates with free circumferential edge and free or rigidly constrained V-notches (Leissa et al. 1993; McGee et al. 1995). The present paper summarizes first-of-the-kind studies on the free vibrations of thin plates having free circular edges and with three other combinations of clamped, simply supported or free straight edges which may occur along the notch, including stress singularity effects at the sharp vertex corner (see Fig. 1). The relative depth of the notch is defined as $(a-c)/a$, and the notch angle is defined as $(360°-\alpha)$. For a very small notch angle (say, one degree or less), the notch may be regarded as a constrained crack. For $c/a=0$, the special case of a sectorial plate with constrained radial edges and free circumferential edge is formed. No published vibration data is available for such sectorial plates with re-entrant angles ($\alpha>180°$) or for the special case of a semicircular plate ($\alpha=180°$), albeit a substantial amount of data exist for salient angles ($\alpha<180°$).

The Ritz method is adopted with the transverse displacement field approximated as a complete set of admissible algebraic-trigonometric polynomials in conjunction with an admissible set of corner functions that exactly model the singular vibratory moments which exist at the vertices of corner angles (α) which exceed 180° (Williams 1951; Huang 1991). The first set guarantees convergence to exact frequencies as sufficient terms are retained. The second set substantially accelerates the convergence of frequencies, which is demonstrated through several convergence studies summarized herein. Reported in this paper is an accurate database of nondimensional frequencies showing the effects of changing relative notch depth $(a-c)/a$ and corner angle α. To fully ascertain the significance of the stress singularities existing in the title problem, normalized contour plots of the vibratory transverse displacements are studied for plates having notch

[1]Professor and Chair, Dept. of Civil and Environmental Engineering and Geodetic Sciences, 470 Hitchcock Hall, 2070 Neil Ave., Columbus, OH 43210. E-mail: mcgee.1@osu.edu

[2]Professor, Dept. of Aerospace Engineering, Applied Mechanics, and Aviation, The Ohio State Univ., Columbus, OH 43210.

[3]Assistant Professor, Dept. of Architectural Engineering, Semyung Univ., Jecheon, Chungbuk 390-711, Korea.

[4]Graduate Research Associate, School of Civil and Environmental Engineering, Georgia Institute of Technology, Atlanta, GA 30332-0355.

Note. Associate Editor: Roger G. Ghanem. Discussion open until December 1, 2003. Separate discussions must be submitted for individual papers. To extend the closing date by one month, a written request must be filed with the ASCE Managing Editor. The manuscript for this paper was submitted for review and possible publication on August 13, 1998; approved on December 6, 2002. This paper is part of the ***Journal of Engineering Mechanics***, Vol. 129, No. 7, July 1, 2003. ©ASCE, ISSN 0733-9399/2003/7-812–822/$18.00.

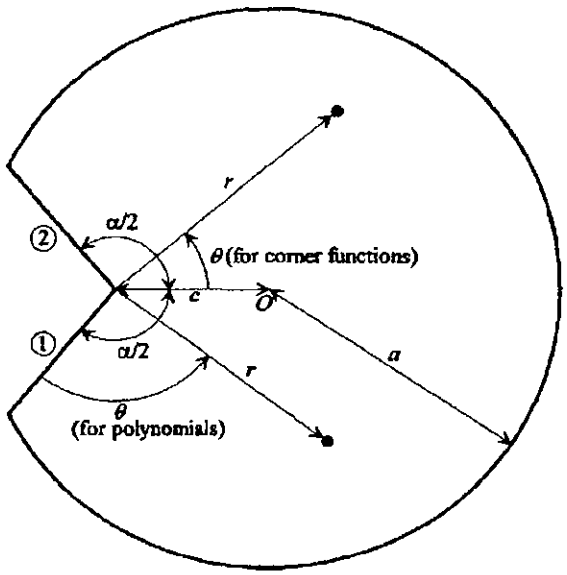

Fig. 1. Geometry of circular plate with V-notch

depths $c/a=0.75$, 0, -0.5, and sector angles $\alpha=90°$, 180°, 270°, 300°, 330°, and 355°.

Methodology

Consider the polar coordinates (r,θ) originating at the vertex of the notch of a circular plate of radius, a, shown in Fig. 1. The transverse motion w of the plate is assumed to vibrate simple harmonically, as follows:

$$w(r,\theta,t)=W(r,\theta)\sin\omega t \tag{1}$$

where t=time; and ω=circular frequency of vibration. In using the Ritz method, one requires the maximum values of potential energy (which is strain energy in this situation) and kinetic energy which occur during a cycle of vibratory motion.

The maximum strain energy V_{max} in the plate due to bending in a vibratory cycle is

$$V_{max}=\frac{D}{2}\int\int_A[(\chi_r+\chi_\theta)^2-2(1-\nu)(\chi_r\chi_\theta-\chi_{r\theta}^2)]dA \tag{2}$$

where $dA=rdrd\theta$; $D=Eh^3/12(1-\nu^2)$=flexural rigidity; h=plate thickness; E=Young's modulus; ν=Poisson's ratio; and χ_r, χ_θ, and $\chi_{r\theta}$=maximum bending and twisting curvatures [$\sin\omega t=1$ assumed in Eq. (1)]

$$\chi_r=\frac{\partial^2 W}{\partial r^2},\quad \chi_\theta=\frac{1}{r}\frac{\partial W}{\partial r}+\frac{1}{r^2}\frac{\partial^2 W}{\partial\theta^2},\quad \chi_{r\theta}=\frac{\partial}{\partial r}\left(\frac{1}{r}\frac{\partial W}{\partial\theta}\right) \tag{3}$$

The maximum kinetic energy is

$$T_{max}=\frac{\rho\omega^2}{2}\int\int_A W^2 dA \tag{4}$$

where ρ=mass per unit area of the plate.

The plates studied in this work all have their circular edges free, and boundary conditions along the straight edges ($\theta=\pm\alpha/2$ in Fig. 2) which are clamped, simply supported, or free. The latter boundary conditions are labeled accordingly as CF, CS, or SF. Displacement trial functions are assumed as the sum of two finite sets: $W=W_p+W_c$, where W_p are algebraic-trigonometric polynomials and W_c are corner functions. No symmetry exists for the CF, CS, and SF plates examined here. Thus, the admissible polynomials are written as

$$W_p=g(r,\theta)\left(\sum_{m=0,2,4}^{M_1}\sum_{n=0,2,4}^{m}A_{mn}r^m\cos n\theta+\sum_{m=1,3,5}^{M_2}\sum_{n=1,3,5}^{m}A_{mn}r^m\cos n\theta+\sum_{m=2,4}^{M_3}\sum_{n=2,4}^{m}B_{mn}r^m\sin n\theta+\sum_{m=1,3,5}^{M_4}\sum_{n=1,3,5}^{m}B_{mn}r^m\sin n\theta\right) \tag{5}$$

in which for the

$$\text{CF plate:}\quad g(r,\theta)=(r/a)^2(\theta/\alpha)^2 \tag{6a}$$

$$\text{CS plate:}\quad g(r,\theta)=(r/a)^2(\theta/\alpha)[(\theta/\alpha)-1]^2 \tag{6b}$$

$$\text{SF plate:}\quad g(r,\theta)=(r/a)^2(\theta/\alpha) \tag{6c}$$

In Eqs. (6), $g(r,\theta)$ is defined to satisfy the essential boundary conditions along the radial edges 1–2 (see Fig. 1). In Eq. (5), A_{mn} and B_{mn} are arbitrary coefficients, and the values of m and n have been specially chosen to eliminate those terms which yield undesirable singularities at $r=0$, and yet, preserve the mathematical completeness of the resulting series as sufficient terms are retained. Thus, convergence to the exact frequencies is guaranteed when the series is employed in the present Ritz procedure.

The displacement polynomial Eq. (5) should, in principle, be

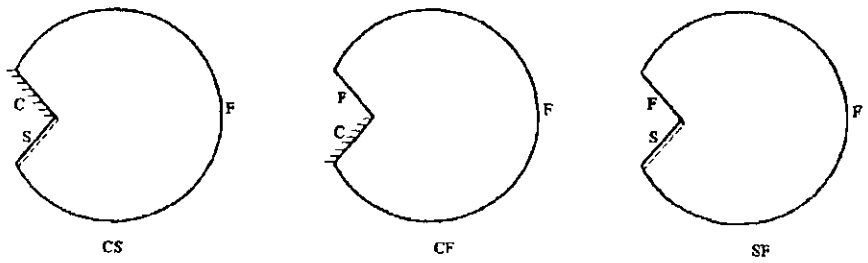

Fig. 2. Circular plates with clamped-hinged, clamped-free, and hinged-free V-notch

capable of yielding accurate frequencies. However, the number of terms required may be computationally prohibitive. This problem is alleviated by augmentation of the complete polynomial set with admissible *corner functions*, which introduce the proper singular vibratory moments at the vertex corner formed by the V-notch radial edges (Fig. 1). The set of corner functions is taken as

$$W_c = \sum_{k=1}^{K} C_k W_{c_k}^* \tag{7}$$

where C_k=arbitrary coefficients; and $W_{c_k}^*$=solutions of the fourth-order biharmonic, static equilibrium equation for bending of plates at acute corner angles (Williams 1951)

$$W_{c_k}^* = r^{\lambda_k+1}[a_k \sin(\lambda_k+1)\theta + b_k \cos(\lambda_k+1)\theta + c_k \sin(\lambda_k-1)\theta + d_k \cos(\lambda_k-1)\theta] \tag{8}$$

The boundary conditions along a representative radial edge $\theta=\alpha/2$ may be clamped {i.e., $W(r,\alpha/2)=(1/r)[\partial W(r,\alpha/2)/\partial\theta]=0$}, simply supported [i.e., $W(r,\alpha/2)=M_r(r,\alpha/2)=0$], or free [i.e., $V_r(r,\alpha/2)=M_r(r,\alpha/2)=0$], where M_r and V_r are the usual radial moment and shear force defined elsewhere (Leissa 1969). These conditions are used in Eq. (8) to construct a set of algebraic equations from which the values λ_k are obtained as roots of the vanishing determinants.

Satisfaction of the *hinged-free* (S-F) radial edge conditions results in the following characteristic equation for the λ_k:

$$\sin 2\lambda_k\alpha = \frac{\nu-1}{3+\nu}\lambda_k \sin 2\alpha \tag{9}$$

The corresponding S-F corner function is

$$W_{c_k}^*(r,\theta) = r^{\lambda_k+1}[\sin(\lambda_k+1)\theta - \gamma_{1_k}\cos(\lambda_k+1)\theta - \gamma_{2_k}\sin(\lambda_k-1)\theta + \gamma_{3_k}\cos(\lambda_k-1)\theta] \tag{10}$$

where

$$\gamma_{1_k} = \frac{\sin(\lambda_k+1)\alpha/2}{\cos(\lambda_k+1)\alpha/2} \tag{11a}$$

$$\gamma_{2_k} = \frac{(\lambda_k+1)(\nu-1)}{\lambda_k(\nu-1)+(3+\nu)}\frac{\sin(\lambda_k+1)\alpha/2}{\sin(\lambda_k-1)\alpha/2} \tag{11b}$$

$$\gamma_{3_k} = \frac{(\lambda_k+1)(\nu-1)}{\lambda_k(\nu-1)+(3+\nu)}\frac{\sin(\lambda_k+1)\alpha/2}{\cos(\lambda_k-1)\alpha/2} \tag{11c}$$

Imposition of the *hinged-clamped* (S-C) radial edge conditions yields the characteristic equation for the λ_k

$$\sin 2\lambda_k\alpha = \frac{\nu-1}{3+\nu}\lambda_k \sin 2\alpha \tag{12}$$

and the corresponding S-C corner function

$$W_{c_k}^*(r,\theta) = r^{\lambda_k+1}\left[\sin(\lambda_k+1)\theta - \frac{\sin(\lambda_k+1)\alpha/2}{\cos(\lambda_k+1)\alpha/2}\cos(\lambda_k+1)\theta - \frac{\sin(\lambda_k+1)\alpha/2}{\sin(\lambda_k-1)\alpha/2}\sin(\lambda_k-1)\theta + \frac{\sin(\lambda_k+1)\alpha/2}{\cos(\lambda_k-1)\alpha/2}\cos(\lambda_k-1)\theta\right] \tag{13}$$

Finally, the characteristic equation in λ_k for the *clamped-free* (C-F) radial edges is

$$\sin^2\lambda_k\alpha = \frac{4}{(1-\nu)(3+\nu)} - \frac{1-\nu}{3+\nu}\lambda_k^2\sin^2\alpha \tag{14}$$

and the associated C-F corner function is

$$W_{c_k}^*(r,\theta) = r^{\lambda_k+1}[\sin(\lambda_k+1)\theta + \zeta_{1_k}\cos(\lambda_k+1)\theta + \zeta_{2_k}\sin(\lambda_k-1)\theta + \zeta_{3_k}\cos(\lambda_k-1)\theta] \tag{15}$$

with

$$\zeta_{1_k} = \frac{\mu_{1_k}}{\delta_k}, \quad \zeta_{2_k} = \frac{\mu_{2_k}}{\delta_k}, \quad \zeta_{3_k} = \frac{\mu_{3_k}}{\delta_k} \tag{16a}$$

$$\mu_{1_k} = (\lambda_k-1)\eta_{2_k}\sin(\lambda_k+1)\frac{\alpha}{2} - (\lambda_k+1)\eta_{1_k}\cos(\lambda_k+1)\frac{\alpha}{2}\sin(\lambda_k-1)\alpha + (\lambda_k-1)\eta_{1_k}\sin(\lambda_k+1)\frac{\alpha}{2}\cos(\lambda_k-1)\alpha \tag{16b}$$

$$\mu_{2_k} = (\lambda_k+1)\left[\eta_{1_k}\cos(\lambda_k-1)\frac{\alpha}{2} - \eta_{2_k}\cos(\lambda_k-1)\frac{\alpha}{2}\cos(\lambda_k+1)\alpha - \eta_{3_k}\sin(\lambda_k-1)\frac{\alpha}{2}\sin(\lambda_k+1)\alpha\right] \tag{16c}$$

$$\mu_{3_k} = (\lambda_k+1)\left[\eta_{1_k}\sin(\lambda_k-1)\frac{\alpha}{2} + \eta_{2_k}\sin(\lambda_k-1)\frac{\alpha}{2}\cos(\lambda_k+1)\alpha - \eta_{3_k}\cos(\lambda_k-1)\frac{\alpha}{2}\sin(\lambda_k+1)\alpha\right] \tag{16d}$$

$$\delta_k = (\lambda_k-1)\eta_{2_k}\cos(\lambda_k+1)\frac{\alpha}{2} - (\lambda_k+1)\eta_{1_k}\sin(\lambda_k+1)\frac{\alpha}{2}\sin(\lambda_k-1)\alpha - (\lambda_k-1)\eta_{1_k}\cos(\lambda_k+1)\frac{\alpha}{2}\cos(\lambda_k-1)\alpha \tag{16e}$$

in which

$$\eta_{1_k} = \lambda_k(\nu-1)+(3+\nu), \quad \eta_{2_k} = (\lambda_k+1)(\nu-1)$$

$$\eta_{3_k} = (\lambda_k-1)(\nu-1) \tag{16f}$$

Some of the λ_k obtained from Eqs. (9), (12), and (14) may be complex numbers, and thus, result in complex corner functions. In such cases, both the real and imaginary parts are used as independent functions in the present Ritz procedure. The required area integrals in the dynamical energy Eqs. (2) and (4) are performed numerically, except in the special case of a sectorial plate ($c/a=0$), where exact integrals are tractable when λ_k is real.

Substituting Eqs. (5)–(8), (10), (11), (13), (15), and (16) into Eqs. (2)–(4) and using the frequency minimizing equations

$$\frac{\partial}{\partial A_{mn}}(V_{\max}-T_{\max})=0, \quad \frac{\partial}{\partial B_{mn}}(V_{\max}-T_{\max})=0, \quad \frac{\partial}{\partial C_k}(V_{\max}-T_{\max})=0 \tag{17}$$

yields a set of homogeneous algebraic equations involving the coefficients A_{mn} (or B_{mn}) and C_k.

The roots of the vanishing determinant of these equations are a set of eigenvalues, which are expressed in terms of the nondimen-

sional frequency parameter $\omega a^2\sqrt{\rho/D}$ commonly used in the plate vibration literature. Eigenvectors involving the coefficients A_{mn}, B_{mn}, and C_k are determined in the usual manner by substituting the eigenvalues back into the homogeneous equations. Normalized contours of the associated mode shapes may be depicted on a $r-\theta$ grid in the sector plate domain, once the eigenvectors are substituted into Eqs. (5) and (7).

Convergence Studies

Addressed in this section is the important question of the convergence rate of V-notched circular plate frequencies, as various numbers of the assumed algebraic-trigonometric polynomials and corner functions are retained. All of the results shown in the present and following sections are for materials having a Poisson's ratio (ν) equal to 0.3. Numerical calculations of all vibratory frequencies and mode shapes were performed on an IBM/RS-6000 970 powerserver with an IBM/RS-6000 340 workstation cluster using double precision (14 significant figure) arithmetic.

Shown in Tables 1–3 are the first six nondimensional frequencies $\omega a^2\sqrt{\rho/D}$ for representative CS, CF, and SF V-notched plates ($\alpha=330°$, $c/a=0$) with free circular edges. Numerical results are shown as 40, 60, 84, and 112 polynomial terms are retained in Eq. (5), in conjunction with 0, 1, 5, 10, 15, and 20 corner functions employed in Eq. (7). As can be seen in Table 1, the lowest-frequency mode of the CS plate converges very slowly as the number of polynomial terms (W_p) is increased with no corner functions. Adding a single corner function improves convergence substantially. That is, the trial set using only a single corner function (corresponding to the lowest λ_k) along with as little as 40 polynomials yields an upper bound $\omega a^2\sqrt{\rho/D}$ value which is much lower than those shown in the first row of data. One can clearly see that by adding the first ten corner functions to as few as 60 polynomials yields the converged value of 2.1315, which is exact to five significant figures.

For the CF and SF radial edge conditions, Tables 2 and 3 show similar levels of convergence accuracy in the $\omega a^2\sqrt{\rho/D}$ values achieved by using hybrid trial sets of admissible polynomials and corner functions. Further data using other numbers of corner functions have shown that the frequencies obtained with 20 corner functions have converged to five significant figures. More detailed, similar convergence studies when the interior straight edges are both free may also be seen in Leissa et al. (1993), and for clamped edges can be seen in McGee et al. (1995).

A slight deterioration in the convergence of $\omega a^2\sqrt{\rho/D}$ may occur for large W_p+W_c, which is attributed to the onset of matrix ill-conditioning due to round-off errors. It should be noted that the associated eigenvalue problem is positive definite, and thus, the frequency data shown in Tables 1–3 was obtained by using a QL algorithm combined with Cholesky factorization (Stewart 1970; Stoer and Bulirsch 1980). For large W_p+W_c, however, the mass operator employed in the above QL algorithm may become ill-conditioned. No such ill-conditioning was encountered in computing the first six nondimensional frequencies (converged to five significant figures) shown in Tables 1–3. Although not compared in Tables 1–3 for the sake of brevity, a larger notch angle ($\alpha<330°$) does not degrade the overall convergence rate and accuracy of frequencies. Furthermore, the convergence is improved to a small degree for a sectorial plate ($c/a=0$) having a large notch angle rather than a small one. For a shallow notched plate ($c/a=0.75$), one may encounter somewhat further deterioration in the convergence of $\omega a^2\sqrt{\rho/D}$ at large W_p+W_c, which is attributed to the onset of ill-conditioning.

Table 1. Convergence of Frequency Parameters $\omega a^2\sqrt{\rho/D}$ for Secorial Plate with Clamped-Simply Supported Radial Edges and Free Circumferential Edge ($\alpha=330°$, $c/a=0$)

Mode number	Number of corner functions	Total number of terms in W_p			
		40	60	84	112
1	0	2.8672	2.7749	2.7081	2.6572
	1	2.1524	2.1484	2.1457	2.1437
	5	2.1318	2.1316	2.1316	2.1315
	10	2.1316	2.1315	2.1315	2.1315
	15	2.1316	2.1315	2.1315	2.1315
	20	2.1316	2.1315	2.1315	2.1315
2	0	3.3672	3.3222	3.2932	3.2729
	1	3.3416	3.3024	3.2768	3.2589
	5	3.1598	3.1596	3.1595	3.1595
	10	3.1594	3.1594	3.1594	3.1594
	15	3.1594	3.1594	3.1594	3.1594
	20	3.1594	3.1594	3.1594	3.1594
3	0	5.5483	5.1990	5.0095	4.8941
	1	5.2471	5.1292	4.9649	4.8635
	5	4.5371	4.5357	4.5351	4.5348
	10	4.5360	4.5352	4.5349	4.5347
	15	4.5357	4.5331	4.5348	4.5347
	20	4.5355	4.5331	4.5348	4.5347
4	0	7.8654	7.7452	7.6934	7.6668
	1	7.8543	7.7412	7.6915	7.6657
	5	7.6228	7.6171	7.6145	7.6132
	10	7.6144	7.6126	7.6116	7.6112
	15	7.6131	7.6121	7.6114	7.6111
	20	7.6129	7.6119	7.6114	7.6111
5	0	12.170	11.801	11.658	11.593
	1	12.160	11.795	11.653	11.589
	5	11.730	11.618	11.568	11.543
	10	11.509	11.506	11.504	11.503
	15	11.506	11.505	11.504	11.503
	20	11.506	11.504	11.504	11.503
6	0	16.388	16.216	16.163	16.144
	1	16.387	16.216	16.163	16.144
	5	16.277	16.182	16.149	16.136
	10	16.143	16.130	16.125	16.122
	15	16.127	16.124	16.122	16.121
	20	16.126	16.123	16.122	16.121

Frequencies and Mode Shapes

Table 4 summarizes the results of extensive convergence studies of the least upper bound frequency parameters $\omega a^2\sqrt{\rho/D}$ for the first three modes of the CS, CF, and SF plates with increasing sector angles (decreasing notch angles), α(or $360°-\alpha$) $=90°(270°)$, $180°(180°)$, $270°(90°)$, $300°(60°)$, $330°(30°)$, $350°(10°)$, $355°(5°)$, and $359°(1°)$, and with increasing notch depths $c/a=0.75$, 0.5, 0, and -0.5. Depicted in Fig. 3 are four typical plate configurations which were analyzed to construct the summary of results in Table 4. These plate configurations are distinguished by their notch depths, ranging from a shallow notch

Table 2. Convergence of Frequency Parameters $\omega a^2\sqrt{\rho/D}$ for Secorial Plate with Clamped-Free Radial Edges and Free Circumferential Edge ($\alpha=330°$, $c/a=0$)

Mode number	Number of corner functions	Total number of terms in W_p			
		40	60	84	112
	0	3.4196	3.2195	3.0669	2.9496
	1	2.2914	2.2818	2.2731	2.2652
1	5	1.8256	1.8241	1.8231	1.8224
	10	1.8202	1.8201	1.8200	1.8199
	15	1.8199	1.8199	1.8198	1.8198
	20	1.8198	1.8198	1.8198	1.8198
	0	4.0346	3.7586	3.5883	3.4689
	1	3.4196	3.2286	3.0912	2.9884
2	5	2.3504	2.3489	2.3479	2.3473
	10	2.3463	2.3460	2.3458	2.3456
	15	2.3455	2.3454	2.3454	2.3453
	20	2.3454	2.3453	2.3453	2.3452
	0	5.3247	4.9153	4.6625	4.4865
	1	5.1654	4.7988	4.5765	4.4224
3	5	3.6251	3.6155	3.6092	3.6050
	10	3.5933	3.5924	3.5918	3.5913
	15	3.5907	3.5905	3.5904	3.5902
	20	3.5903	3.5902	3.5901	3.5900
	0	7.8597	7.2315	6.8576	6.6014
	1	7.8594	7.2314	6.8575	6.6012
4	5	5.7145	5.6877	5.6705	5.6593
	10	5.6447	5.6389	5.6353	5.6328
	15	5.6300	5.6293	5.6287	6.6282
	20	5.6286	5.6282	5.6278	5.6275
	0	11.615	10.696	10.177	9.8390
	1	11.440	10.542	10.051	9.7373
5	5	9.4602	9.2476	9.1361	9.0704
	10	8.9087	8.8921	8.8833	8.8777
	15	8.8714	8.8697	8.8688	8.8679
	20	8.8687	8.8680	8.8674	8.8669
	0	15.728	14.711	14.169	13.824
	1	15.723	14.711	14.166	13.817
6	5	14.626	13.843	13.477	13.278
	10	12.995	12.933	12.903	12.887
	15	12.875	12.868	12.866	12.864
	20	12.865	12.863	12.862	12.862

Table 3. Convergence of Frequency Parameters $\omega a^2\sqrt{\rho/D}$ for Secorial Plate with Simply Supported-Free Radial Edges and Free Circumferential Edge ($\alpha=330°$, $c/a=0$)

Mode number	Number of corner functions	Total number of terms in W_p			
		40	60	84	112
	0	3.8253	3.6852	3.5488	3.4162
	1	1.9753	1.9744	1.9739	1.9736
1	5	1.9732	1.9730	1.9729	1.9729
	10	1.9729	1.9728	1.9728	1.9728
	15	1.9728	1.9728	1.9728	1.9728
	20	1.9728	1.9728	1.9728	1.9728
	0	4.1379	3.8930	3.7336	3.6332
	1	3.8636	3.7604	3.6792	3.6123
2	5	2.9967	2.9956	2.9950	2.9947
	10	2.9943	2.9943	2.9943	2.9943
	15	2.9943	2.9943	2.9943	2.9943
	20	2.9943	2.9943	2.9943	2.9943
	0	5.2421	4.9816	4.8444	4.7669
	1	5.0401	4.8985	4.8089	4.7512
3	5	4.5848	4.5837	4.5830	4.5827
	10	4.5824	4.5823	4.5823	4.5823
	15	4.5823	4.5823	4.5823	4.5823
	20	4.5823	4.5823	4.5823	4.5823
	0	9.2999	8.5781	8.2800	8.1188
	1	9.2231	8.5603	8.2568	8.0935
4	5	7.7695	7.7569	7.7501	7.7468
	10	7.7440	7.7436	7.7435	7.7434
	15	7.7435	7.7434	7.7434	7.7434
	20	7.7434	7.7434	7.7434	7.7434
	0	12.041	11.872	11.786	11.740
	1	12.041	11.868	11.775	11.724
5	5	11.631	11.628	11.626	11.625
	10	11.626	11.625	11.624	11.624
	15	11.625	11.624	11.624	11.624
	20	11.624	11.624	11.624	11.624
	0	17.581	16.741	16.451	16.326
	1	17.422	16.623	16.342	16.218
6	5	16.677	16.253	16.105	16.050
	10	16.009	16.005	16.004	16.003
	15	16.003	16.003	16.003	16.003
	20	16.003	16.003	16.003	16.003

($c/a=0.75$) to an extremely deep notch ($c/a=-0.5$). All frequency results are converged to the five significant figures shown in Table 4. Hence, Table 4 provides a very accurate database of frequencies for V-notched circular plates having various radial edge conditions and notch angles against which future results using experimental or other theoretical methods (such as finite element analysis) may be compared.

For the range of α examined in Table 4, it can be seen that in some instances $\omega a^2\sqrt{\rho/D}$ exhibits either an increase before a decrease, or vice versa, as the notch depth increases (i.e., c/a decreases). The frequency variability with notch depth is exhibited in all modes, more so in the lower ranges of α than in the higher ones. It should be noted that the CF plates essentially vibrate as cantilevered ones, rigidly clamped along one radial edge, whereas the fundamental (lowest frequency) mode of the SF plates is a rigid body rotation about the hinged radial edge (at zero frequency, which is not shown in Table 4). Naturally, the plates with $\alpha=90°$ or 180° (semicircular) do not form a V-notch. Nonetheless, the frequency data for $\alpha=90°$ do delineate some interesting special cases of plates with decreasing c/a (see Fig. 4) for which no previously published frequency results are known to exist. For $350°\leq\alpha\leq359°$, the range in $\omega a^2\sqrt{\rho/D}$ due to the notch effect (decreasing c/a) is comparatively less, as one observes the various ranges in $\omega a^2\sqrt{\rho/D}$ with decreasing c/a over all α.

Table 4. Fundamental Frequency Parameters $\omega a^2\sqrt{\rho/D}$ for Circular Plates Having Various Radial Edge Conditions and Free Circumferential Edge

Case	Mode number	c/a	α (deg)							
			90	180	270	300	330	350	355	359
		0.75	2.9070	1.0275	1.0115	0.9998	0.9583	0.9240	0.9153	0.9084
	1	0.5	4.0672	1.4177	1.4186	1.4548	1.4133	1.3577	1.3435	1.3322
		0	9.3413	2.9913	2.5161	2.3670	2.1315	2.0010	1.9748	1.9557
		−0.5	37.116	9.7790	4.0651	2.9258	2.1458	1.7862	1.7125	1.6576
		0.75	8.9921	2.6876	1.6105	1.4986	1.4501	1.4450	1.4459	1.4472
CS	2	0.5	12.383	3.6942	2.0337	1.8206	1.7403	1.7402	1.7436	1.7470
		0	27.458	7.3860	3.5591	3.2274	3.1594	3.1535	3.1509	3.1475
		−0.5	104.63	23.132	10.207	7.7956	5.7452	4.7323	4.5170	4.3546
		0.75	13.987	5.8987	4.3515	4.3043	4.3179	4.3371	4.3418	4.3453
	3	0.5	18.999	7.8816	4.9149	4.5822	4.4118	4.3645	4.3593	4.3568
		0	41.896	14.806	6.7273	5.4633	4.5347	4.0615	3.9605	3.8848
		−0.5	160.15	39.852	12.488	9.9622	8.0305	6.8415	6.5738	6.3694
		0.75	1.7092	1.0111	0.8635	0.8447	0.8312	0.8232	0.8214	0.8200
	1	0.5	2.2297	1.3637	1.2130	1.1945	1.1826	1.1754	1.1735	1.1718
		0	4.4927	2.4769	2.1656	1.9580	1.8198	1.7637	1.7534	1.7460
		−0.5	15.483	5.1297	1.8718	1.4190	1.1476	1.0327	1.0100	0.9933
		0.75	4.5592	2.0806	1.5674	1.4833	1.4212	1.3885	1.3815	1.3762
CF	2	0.5	6.1723	2.5476	1.8967	1.7843	1.6959	1.6484	1.6380	1.6301
		0	13.571	4.1541	2.4793	2.4349	2.3452	2.2403	2.2100	2.1850
		−0.5	52.030	12.289	5.3052	3.9840	3.0048	2.5251	2.4237	2.3474
		0.75	9.5867	4.8819	4.2919	4.2615	4.2544	4.2547	4.2552	4.2556
	3	0.5	12.557	5.7698	4.4856	4.3814	4.3323	4.3171	4.3148	4.3133
		0	24.895	9.6393	4.6903	3.9968	3.5900	3.4492	3.4263	3.4109
		−0.5	83.101	26.490	9.9304	7.7371	5.8204	4.8055	4.5859	4.4195
		0.75	3.4651	1.7636	1.1578	0.9735	0.8242	0.7675	0.7607	0.7575
	1	0.5	4.5616	2.0108	1.3968	1.2458	1.1319	1.0886	1.0828	1.0796
		0	9.4966	2.7664	2.2165	2.2117	1.9728	1.7918	1.7520	1.7222
		−0.5	34.312	5.1867	3.5685	2.3630	1.5186	1.1556	1.0876	1.0395
		0.75	6.9781	4.2979	3.9799	4.0283	4.1285	4.1954	4.2098	4.2202
SF	2	0.5	9.0402	5.0360	4.1387	4.0705	4.0872	4.1206	4.1312	4.1401
		0	18.055	7.6352	3.5006	3.0320	2.9943	3.0431	3.0543	3.0621
		−0.5	61.863	17.542	4.8946	4.1863	3.2557	2.7005	2.5782	2.4853
		0.75	11.880	7.6039	6.0297	5.7083	5.4639	5.3544	5.3358	5.3239
	3	0.5	14.979	8.9503	6.0221	5.5638	5.2558	5.1138	5.0856	5.0651
		0	29.179	14.852	6.8796	5.5628	4.5823	4.0677	3.9548	3.8691
		−0.5	100.62	34.998	10.298	8.3440	7.1815	6.3205	6.1058	5.9378

Note: CS=clamped-hinged; CF=clamped-free; and SF=hinged-free.

For constant c/a, one can see in Table 4 that there is, for the most part, a decreasing trend in $\omega a^2\sqrt{\rho/D}$ for the first three modes, as α increases. Physically speaking, one can even expect a monotonic decrease in $\omega a^2\sqrt{\rho/D}$ versus α, for α>360° (i.e., a very thin plate wrapped under itself) due to the increasing strength of the singular moments at $r=0$. A closer scrutiny of the frequency data does reveal a number of slight exceptions to this overall trend, which would be too numerous and tedious to explain here. However in Table 4, e.g., Mode 3 for CS ($c/a=0.75$) and Mode 2 for SF ($c/a=0$), a slight increase in $\omega a^2\sqrt{\rho/D}$ can be seen as α approaches 360°. The frequency results as α approaches 360° are special cases of circular plates having what are described here as a hinged-clamped, clamped-free, or hinged-free radial crack. It is seen in Table 4 that relatively minimal change in $\omega a^2\sqrt{\rho/D}$ with c/a results with either a constrained, sharp V-notch (α=355°) or radial crack (α=359°). Moreover, the frequencies for the sharp notch and the radial crack are seen to be only slightly different.

Normalized contours of the transverse vibratory displacement are shown in Figs. 5–7 for plates having α=90°, 180°, 270°, 300°, 330°, and 355° sector angles, for increasing notch depths of $c/a=0.75$, 0, and −0.5. Increasing the notch depth has a significant effect on the nodal patterns of Modes 1–3 (Note that the node lines are shown in Figs. 5–7 as darker contour lines of zero displacement [$(W/W_{max}=0)$ during vibratory motion]. In addition, increasing the notch depth causes distinct nodal line separations, and noticeable distortions and sharp curvature of the normalized displacement contours (W/W_{max}) near the notch vertex, more so to a small degree in the higher modes than in the lower ones. The contour plots of Figs. 5–7 are normalized with

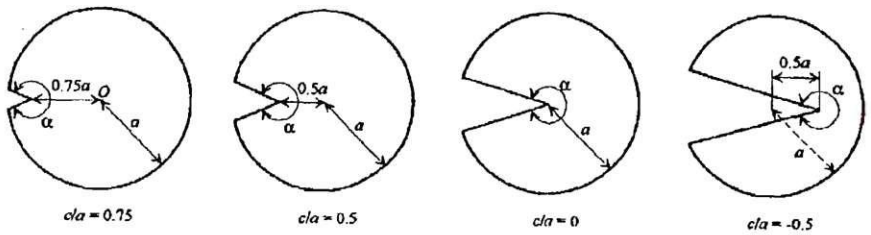

Fig. 3. V-notched circular plates with various depths

respect to the maximum transverse displacement component(i.e., $-1 \leq W/W_{max} \leq 1$, where the negative values of W/W_{max} are depicted as dashed contour lines in Figs. 5–7, and the nondimensional frequencies shown correspond to the data listed in Table 4).

What is particularly interesting about the subject problem is that the large bending moment stresses in the neighborhood of the vertex of the constrained, sharp notch or crack do indeed significantly influence the nature of the vibratory behavior of circular plates. It is important to emphasize that the singular stresses at the constrained vertex of such sharp notches or cracks can become quite serious during vibration by constituting an origin for crack propagation during fatigue. A reasonable simulation of this propagation effects is shown in the displacement contours of Figs. 5–7. Similar contours of the radial (M_r), circumferential (M_θ), and twisting ($M_{r\theta}$) moments may be obtained from the following:

$$M_r = -D(\chi_r + \nu\chi_\theta), \quad M_\theta = -D(\chi_\theta + \nu\chi_r)$$
$$M_{r\theta} = -D(1-\nu)\chi_{r\theta} \tag{18}$$

Additional studies (the results of which are not shown here) revealed that approximate normalized values of the vibratory moments $-1 \leq (M_r/M_{r_{max}}; M_\theta/M_{\theta_{max}}; M_{r\theta}/M_{r\theta_{max}}) \leq 1$ are highly localized around the vertex of the notch or crack. Since the vibratory moments asymptotically approach infinity in the limit as r approaches zero at the vertex, approximate maximum values of M_r, M_θ, and $M_{r\theta}$ were assumed within a very small radial distance from the sharp corner of the vertex. Given that the moments are indeed infinite at the sharp corner, depictions of these approximate normalized moment variations elsewhere in the plate domains, relatively speaking, were of little interest.

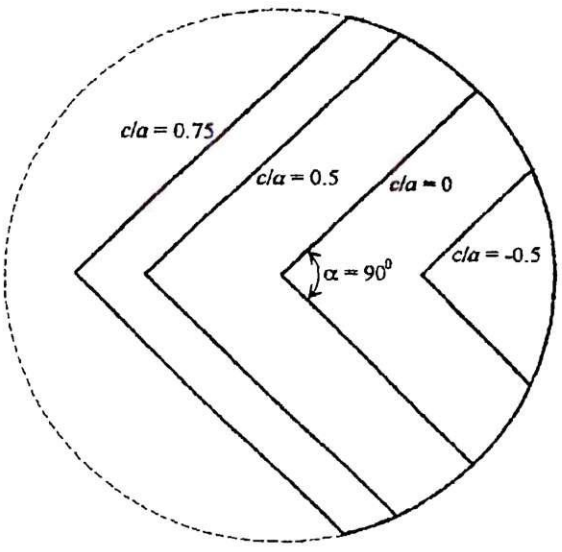

Fig. 4. Plates with $\alpha = 90°$ and various c/a ratios

Concluding Remarks

A Ritz procedure in conjunction with classical thin-plate theory has been developed to obtain highly accurate frequencies and mode shapes for circular plates having a free circumferential edge with clamped-hinged, clamped-free, and hinged-free V-notches or sharp radial cracks. In this approximate procedure, the assumed transverse displacement of the plate consists of a hybrid set of complete algebraic-trigonometric polynomials along with corner functions that account for the proper singular bending moments at the vertex of acute corner angles. The modeling capability of such corner functions has been substantiated through supporting convergence studies of nondimensional frequencies.

Detailed numerical tables have been presented, showing the variations of nondimensional frequencies (accurate to five significant figures) over a wide range of notch depths c/a and vertex angles α. The frequency variability with notch depth is exhibited in all modes, to a larger extent, in the higher ranges of α than in the lower ones. For constant c/a, there is, generally speaking, a decreasing trend in $\omega a^2\sqrt{\rho/D}$ for the first three modes, as α increases, with noticeable variability of $\omega a^2\sqrt{\rho/D}$ with α in the higher modes of plates with notch depths exceeding one-half of the plate radius.

Besides this, some new understanding has been offered here with the previously unpublished mode shapes for circular plates with a constrained V-notch or a sharp radial crack. Generally speaking, for $\alpha > 180°$ highly localized bending moment stresses at the vertex of clamped-free, hinged-clamped, and hinged-free sharp notches or cracks may become detrimental in connection with vibration, by constituting an origin for crack propagation during fatigue. Reinforcement and repair of such crack propagation and growth with a rigid material or hinge may serve to increase the plate resistance somewhat to localized fatigue stresses during lateral vibration. Some fundamental understanding of the effect of these localized stresses on V-notched circular plate dynamics can be obtained through careful examination of the frequency and mode shape data offered herein. What is discerned from these previously unavailable results is that the present method is an effective one for modeling the unbounded vibratory stresses which exist at the sharp corner of constrained V-notches or cracks of circular plates. Finally, the accurate vibration data presented here serves as benchmark values for comparison with data obtained using modern experimental and alternative theoretical approaches.

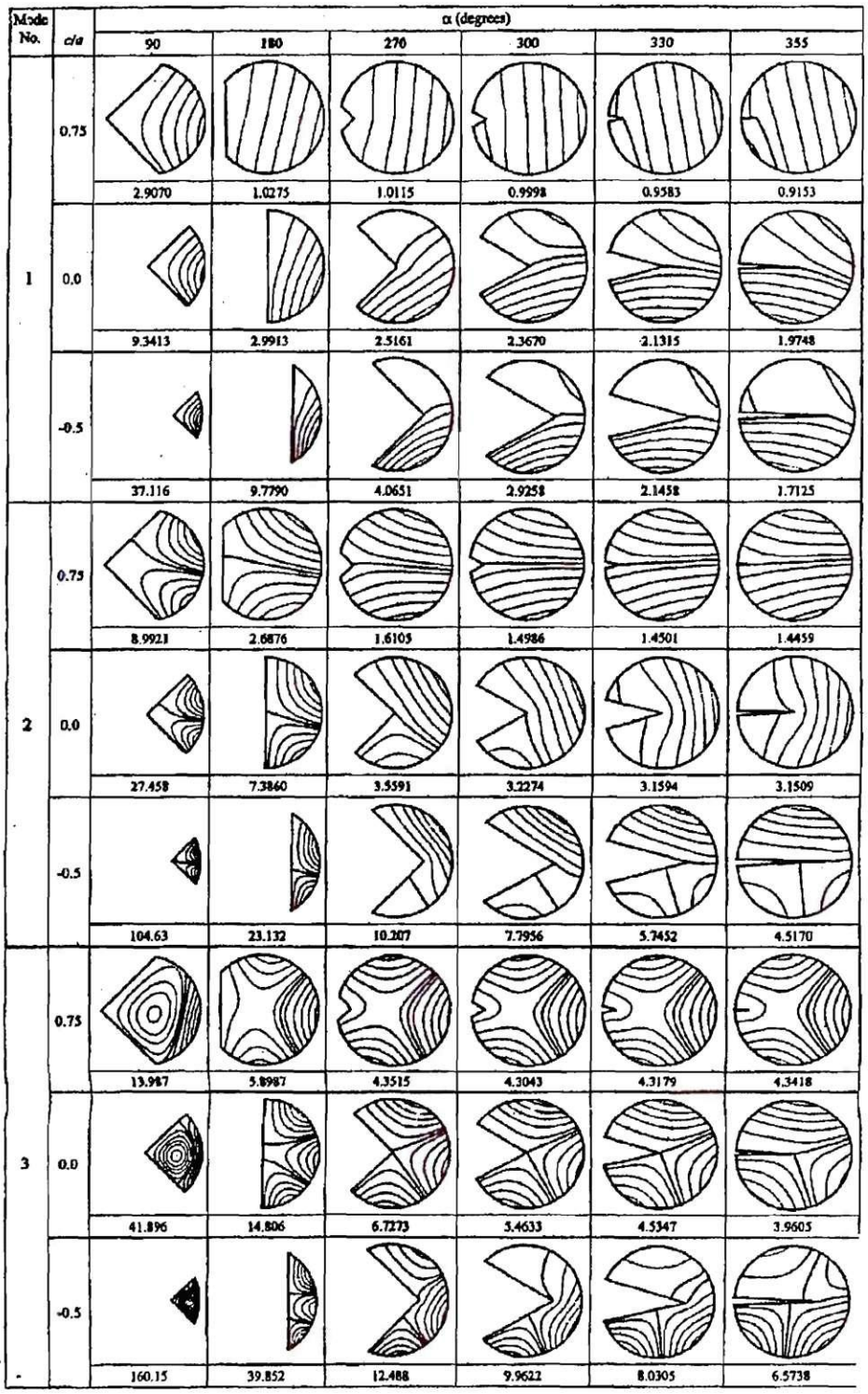

Fig. 5. Normalized transverse displacement contours (W/W_{max}) for CS plates

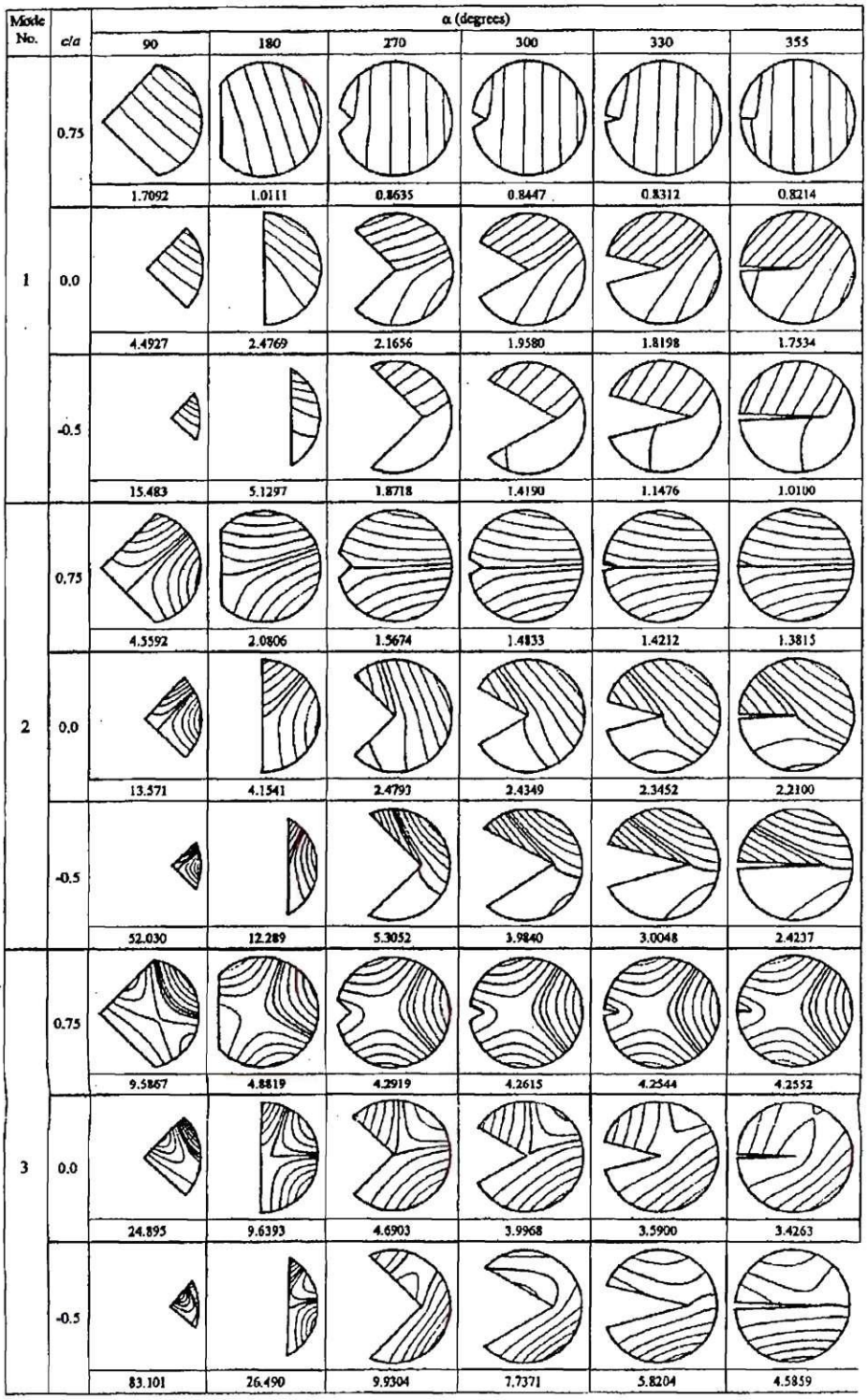

Fig. 6. Normalized transverse displacement contours (W/W_{max}) for CF plates

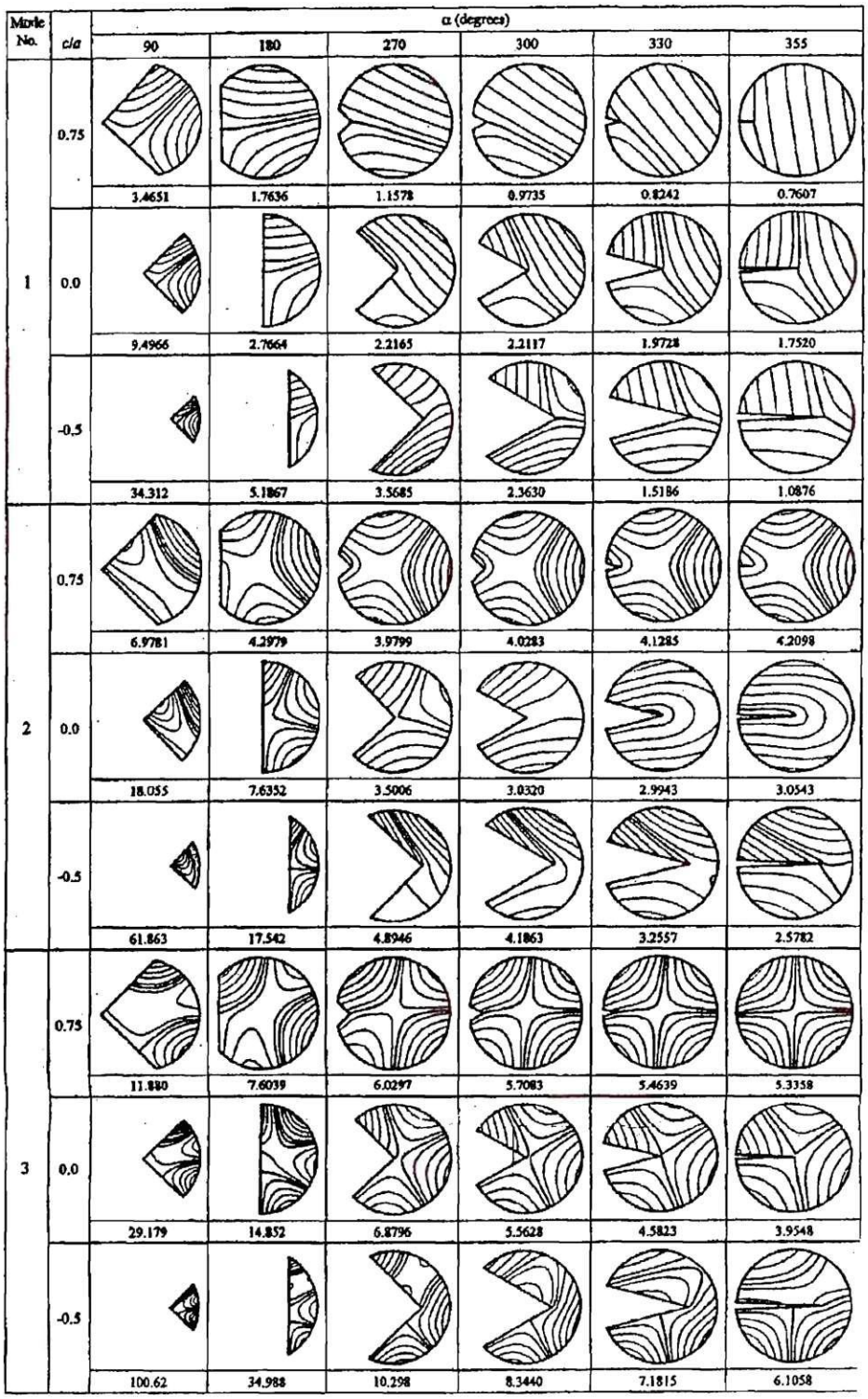

Fig. 7. Normalized transverse displacement contours (W/W_{max}) for SF plates

Acknowledgments

This research was supported by the National Science Foundation, Award Nos MSS-9157972 and CMS-9496202. Portions of this work was completed while the lead writer was on leave as a Martin Luther King Jr. Visiting Associate Professor at the Massachusetts Institute of Technology, Department of Civil and Environmental Engineering.

Notation

The following symbols are used in this paper:

A = plate area;
A_{mn}, B_{mn} = generalized coefficient in Eq. (5);
a = plate radius;
C_k = generalized coefficient in Eqs. (7);
c = notch vertex offset distance (see Fig. 1);
D = plate flexural rigidity;
E = Young's modulus;
g = radial edge equation;
h = plate thickness;
$M_r, M_\theta, M_{r\theta}$ = radial, circumferential, and twisting moments;
r = local polar coordinate at vertex corner;
T_{max} = maximum kinetic energy;
t = time;
V_{max} = maximum strain energy;
V_r = radial shear force;
W_c = corner functions trial series;
W_p = algebraic-trigonometric polynomial trial series;
w = transverse displacement of plate;
$\chi_r, \chi_\theta, \chi_{r\theta}$ = maximum radial, circumferential, and twisting curvatures;
α = corner angle (see Fig. 1);
θ = local polar coordinate at vertex corner.
λ_k = roots of characteristic Eqs. (9), (12), (14);
ν = Poisson's ratio;
ρ = mass density; and
ω = circular frequency of vibration.

References

Eastep, F. E., and Hemming, F. G. (1978). "Estimation of fundamental frequency of noncircular plates with free, circular cutouts." *J. Sound Vib.*, 56, 155–165.

Huang, C. S. (1991). "Singularities in plate vibration problems." PhD dissertation, Ohio State Univ., Columbus, Ohio.

Khurasia, H. B., and Rawtani, S. (1978). "Vibration analysis of circular plates with eccentric hole." *ASME J. Appl. Mech.*, 45(1), 215–217.

Leissa, A. W. (1969). *Vibration of Plates, NASA SP-160.* Washington, D.C., U.S. Government Printing Office (Reprinted by The Acoustical Society of America, 1993).

Leissa, A. W. (1977). "Recent research in plate vibrations: Classical theory." *The shock and vibration digest*, Naval Research Laboratory Washington, D.C., 9(10), 13–24.

Leissa, A. W. (1981). "Plate vibration research, 1976–1980: Classical theory." *The shock and vibration digest*, Naval Research Laboratory Washington, D.C., 13(9), 11–22.

Leissa, A. W. (1987). "Recent studies in plate vibrations: 1981–1985, part I, classical theory." *The shock and vibration digest*, Naval Research Laboratory Washington, D.C., 19(2), 11–18.

Leissa, A. W., McGee, O. G., and Huang, C. S. (1993). "Vibrations of circular plates having V-notches or sharp radial cracks." *J. Sound Vib.*, 161(2), 227–239.

McGee, O. G., Leissa, A. W., Huang, C. S., and Kim, J. W. (1995). "Vibrations of circular plates with clamped V-notches or rigidly constrained radial cracks." *J. Sound Vib.*, 181(2), 185–201.

Nagaya, K. (1977). "Transverse vibration of a plate having an eccentric inner boundary." *ASME J. Appl. Mech.*, 44(1), 165–166.

Nagaya, K. (1979). "Vibration of a viscoelastic plate having a circular outer boundary and an eccentric inner boundary for various edge conditions." *J. Sound Vib.*, 63, 73–85.

Nagaya, K. (1981). "Simplified method for solving problems of vibrating plates of doubly-connected arbitrary shape. I: Derivation of the frequency equation. II: Applications and experiments." *J. Sound Vib.*, 74, 543–551, 553–564.

Nagaya, K. (1983). "Direct method for the determination of eigenfrequencies of arbitrarily-shaped plates." *J. Vibration, Acoustics, Stress and Reliability in Design*, 105(1), 132–136.

Stewart, G. W. (1970). *Introduction to matrix computation*, Academic Press, New York.

Stoer, J., and Bulirsch, R. (1980). *Introduction to numerical analysis*, Springer-Verlag, New York, Article 6.7.

Williams, M. L. (1951). "Surface stress singularities resulting from various boundary conditions in angular corners of plates under bending." *Proc., 1st U.S. National Congress of Applied Mechanics*, Chicago, 325–329.